High-resolution air shower observations with the Square Kilometer Array

S. Buitink,[a,b,*] **J. Bray,**[c] **A. Corstanje,**[a,b] **M. Desmet,**[a] **H. Falcke,**[b,d,e] **K. Gayley,**[f]
B. M. Hare,[d] **J. R. Hörandel,**[a,b,e] **T. Huege,**[a,g] **C. W. James,**[h] **V. B. Jhansi,**[i]
N. Karastathis,[g] **G. K. Krampah,**[a] **P. Mitra,**[a] **K. Mulrey,**[b,e] **B. Neijzen,**[d] **A. Nelles,**[j,k]
H. Pandya,[a] **O. Scholten,**[l,m] **F. Schröder,**[g,n] **R. Spencer,**[c] **K. Terveer,**[k]
S. Thoudam,[i] **G. Trinh,**[o] **S. ter Veen**[d] **and M. Waterson**[p]

[a] *Vrije Universiteit Brussel, Astrophysical Institute, Pleinlaan 2, 1050 Brussels, Belgium*

[b] *Dept. of Astrophysics/IMAPP, Radboud University Nijmegen, P.O. Box 9010, 6500 GL Nijmegen, NL*

[c] *Dept. of Physics and Astronomy, The University of Manchester, UK*

[d] *Netherlands Institute for Radio Astronomy (ASTRON), Postbus 2, 7990 AA Dwingeloo, The Netherlands*

[e] *Nikhef, Science Park Amsterdam, 1098 XG Amsterdam, The Netherlands*

[f] *University of Iowa, Department of Physics and Astronomy, USA*

[g] *Institut für Astroteilchenphysik, Karlsruhe Institute of Technology (KIT), Karlsruhe, Germany*

[h] *Curtin University, International Centre for Radio Astronomy Research, Bentley, WA 6102, Australia*

[i] *Department of Physics, Khalifa University, P.O. Box 127788, Abu Dhabi, United Arab Emirates*

[j] *Deutsches Elektronen-Synchrotron DESY, Platanenallee 6, 15738 Zeuthen, Germany*

[k] *ECAP, Friedrich-Alexander-Universität Erlangen-Nürnberg, 91058 Erlangen, Germany*

[l] *Interuniversity Institute for High-Energy, Vrije Universiteit Brussel, Pleinlaan 2, 1050 Brussels, Belgium*

[m] *University of Groningen, Kapteyn Astronomical Institute, Groningen, 9747 AD, Netherlands*

[n] *Bartol Research Institute, Dept. of Physics and Astronomy, Univ. of Delaware, Newark, DE 19716, USA*

[o] *Dept. of Physics, School of Education, Can Tho University Campus II, Vietnam*

[p] *SKA Observatory, Jodrell Bank, Lower Withington, Macclesfield, SK119FT, UK*

E-mail: stijn.buitink@vub.be

The low-frequency part of the Square Kilometer Array will have an extremely high antenna density of roughly 60.000 antennas within one square kilometer, offering exciting new possibilities for high-resolution studies of air showers. Observing with a frequency band of 50-350 MHz, the SKA will cover the energy range between the knee and the ankle, employing beam forming techniques to reach the lower energies. Using standard techniques, the SKA will reach a resolution on X_{max} of 10 g/cm^2. In addition, the high antenna density allows for the development of new techniques to reconstruct the longitudinal shower development, that can be used to test hadronic interaction models and put additional constraints on the mass composition in the Galactic-extragalactic transition energy range. In this contribution, we review the science case for SKA cosmic-ray detection and the status of the prototype scintillator triggering array.
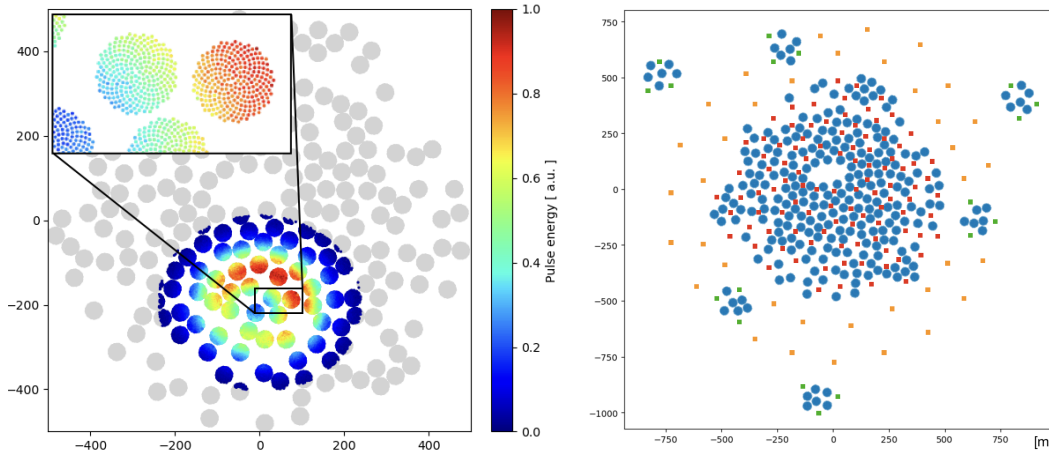
*Speaker

Figure 1: Left: Example of a simulated air shower observation. The SKA consists of stations of 256 antennas each. This radiation pattern is sampled by more than 10.000 antennas. Right: The SKA core plus satellite stations. Each blue circle indicates a station of 256 antennas. The squares indicate the foreseen position of the SKAPA detectors, consisting of a dense core, a ring around the core, and additional decectors near the satellite station.

1. Introduction

The low-frequency part of the Square Kilometre Array will have roughly $60,000$ antennas within an area of one square kilometer. The antennas are omni-directional and have a large bandwidth of $50 - 350$ MHz. This makes the SKA a unique site for radio detection of air showers, offering new reconstruction possibilities that can contribute to cosmic-ray source identification.

The size of the SKA determines the upper limit on the cosmic-ray energy at $\sim 10^{18}$ eV. At lower energies, the strength of the radio signal is the limiting factor. The design and antenna density of the SKA allows for a considerable gain in sensitivity by using beamforming. The lower energy range will lie around 10^{16} eV. This part of the cosmic-ray spectrum, between the knee and ankle, is very complex. It is likely to contain the transition from Galactic to extra-galactic origin. Moreover, it may contain a secondary Galactic component consisting of cosmic-rays that are re-accelerated at the Galactic termination shock or that gain their energy in the strongly magnetized shocks of Wolf-Rayet supernovae [1].

Determining the cosmic-ray mass composition is key to understanding the astrophysics between the knee and ankle. This needs to be measured with high accuracy as some models predict transitions between elements of similar masses. The SKA will achieve a reconstruction resolution on X_{max} that is higher than any other experiment in its energy range. Moreover, new techniques can be developed that allow the reconstruction of the shape of the longitudinal development, putting unique constraints on the primary mass composition.

2. Particle array prototype at MWA

The core of the SKA consists of a densely instrumented circle with a radius of ∼ 500 m and several satellite stations around it, as shown in the right panel of Fig. 1. This map also contains a first design of the layout of the SKA Particle Array (SKAPA). The array will consist of 128 detector units covering the dense core, a ring around the core, and additional detectors near the satellite stations. In the dense region, detector spacing will be roughly 50 m, with exact locations depending on limitations due to the antenna infrastructure.

A first prototype detector was deployed in 2018, and ran stably for a year, after which it was turned off. This detector had four silicon photomultipliers (SiPMs) attached to the four sides of a scintillator slab. The SiPMs were staggered by 50ns to allow discrimination between 1-, 2-, 3-, and 4-fold events. Relative N-fold trigger rates matched those expected from a toy detector model, and were confirmed by measurements in the muon tower at Karlsruhe Institute of Technology. An expected diurnal oscillation in rates of ±30% due to temperature fluctuations was observed, as well as an hourly oscillation of ±10% due to temperature cycling in the power supply [2].

An array of eight particle detectors is now being readied for deployment at the core of the Murchison Widefield Array (MWA). It will consist of eight plastic scintillation detectors, each of two assemblies consisting of two 47.5x47.5x3 cm blocks of scintillator, connected by a wavelength shifter. Each assembly is viewed by two 2x2 arrays of SensL J-Series 6 mm x 6 mm SiPMs, with one connected to the wavelength shifter for maximum sensitivity, and one viewing the scintillator directly for extra dynamic range to high particle fluxes. These assemblies, together with their electronics, are housed in weather-proof aluminium boxes.

Power will be supplied to each detector via a custom 48V power supplies with electronically controlled voltages. This will allow the SiPM voltage to be adjusted to counteract temperature-dependent variation in the gain of the SiPMs. The power supply will be housed in an RFI shielded field cabinet, and delivered via 400 m of shielded cable to each detector.

Data will be returned via ASTRON radio-frequency over fibre (RFoF) modules to the central processing building, approximately 6km distant. It is then fed into the data acquisition board 'Bedlam', developed for the LUNASKA lunar neutrino experiment at Parkes [3]. This FPGA based system will digitise all eight inputs, perform matched filtering for the expected pulse shape (mostly due to the impulse response of the RFoF link), and perform near-real-time analysis to require multiple detectors to trigger above some threshold within the light travel time.

Upon a successful trigger, a message will be sent to the MWA, which buffers 24 1.28 MHz channels for approximately three minutes. An eight second block of data will be returned for further processing, including inversion of the MWA's polyphase filterbank [4]. The array will operate in fully commensal mode, giving an instantaneous bandwidth of 30.72 MHz spread over 80-300 MHz, and nominal 620 deg^2 sky sensitivity at 150 MHz. The design has been chosen to minimise radio-frequency interference in the radio-quiet Murchison Radio-Astronomy Observatory

The eight detectors and power supply have been designed and are being assembled at the University of Manchester; the scintillator has been donated by the KASKADE-Grande Collaboration, centred at Karlsruhe; the data acquisition board was designed and built by CSIRO; while deployment, which is expected to be performed during Q3 2023, will be coordinated by Curtin University.

3. High-resolution shower reconstruction

Air shower radio arrays like LOFAR and AERA employ a reconstruction method that is based on the generation of dedicated sets of Monte Carlo simulations for each observed shower [5]. The showers in such a set share the same geometry and atmospheric profiles, but contain shower-to-shower fluctuations like X_{max} and other characteristics of the evolution. To study the performance of the SKA, radio data was simulated with CORSIKA/CoREAS. The antenna response of the SKALA2 antenna, and random sky noise in the 50-350 MHz range were included in the signal (see [6] and references therein).

The large antenna density and increased bandwidth results in a spectacular improvement in the reconstruction resolution with respects to LOFAR. The core can be reconstructed with a resolution of 50 cm. The energy resolution is 3%, and the resolution on X_{max} is below 8 g/cm^2 [6]. Note that these values do not yet include uncertainties due to the antenna model and the atmosphere, which will likely be the limiting factor on the final performance.

High-resolution observations in the energy range between the knee and the ankle will contribute to the study of the galactic-extragalactic transition region. In addition, these observations will support and enhance other experiments. Currently, there exists tension between the mass composition results of LOFAR [7] and AERA [8]. The SKA can be virtually "downgraded" to either array by selecting an appropriate antenna set and frequency bandwidth. Reconstruction pipelines of different observatories can then be applied to the same shower to test for biases.

In addition, a small portable array of SKA antennas can be transported to different experiments to compare energy scales with reduced systematic uncertainties [9].

4. Mass composition

Broadband radio observations with thousands of antennas simultaneously can offer exciting new possibilities in shower reconstruction. The frequency spectrum of the radio pulse for a given observer position depends on the projected length scales of the shower. Therefore, the radiation pattern on the ground contains information about the shape of the longitudinal development of the shower. To explore the possibility of retrieving this information we have performed a Monte Carlo study. The longitudinal profiles of the simulated shower are fitted to a parametrization found in [10]:

$$N(X) = \exp\left(-\frac{X - X_{max}}{RL}\right)\left(1 - \frac{R}{L}\left(X - X_{max}\right)\right)^{\frac{1}{R^2}},$$ (1)

where N is the number of particles in the shower, and X is the atmospheric depth in g/cm^2. The parameter L scales with the width of the profile and is a measure for the length of the shower, while R is a measure for the asymmetry in the profile shape before and after the shower maximum.

The influence of L on the radio emission has already been observed in LOFAR data. The left panel of Fig. 2 shows the reduced χ^2 of the fit of the measurements to simulated showers as a function of X_{max}. Such curves are used to reconstruct X_{max} by fitting a lower envelope parabola. When color-coding the simulations by their L-value, we can see that the scatter that is often observed correlates strongly with L. This demonstrated that the shape of longitudinal evolution has an observable effect on the radiation.
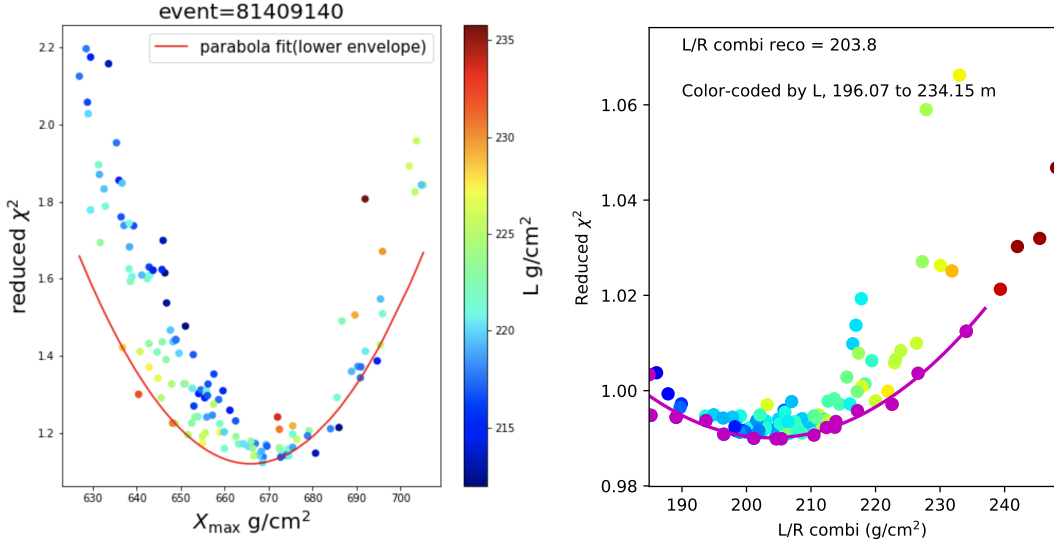
Figure 2: Left: Reconstruction of X_{max} for LOFAR shower (real data). The reduced χ^2 of the fit of the measurements to simulated showers is plotted against the X_{max} of the simulation. The data points are color-coded by their L-value. Right: Reconstruction of a linear combination of R and L for SKA simulations. All simulations shown here have the same X_{max} values.

In the right panel of Fig. 2 each data point is a simulated SKA shower. All showers have almost the same value for X_{max}, but their R and L values differ. It was shown in [6] that a linear combination of L and R can indeed be reconstructed by fitting a parabola.

In a realistic scenario, X_{max} and L and/or R must be reconstructed simultaneously. While this was shown to be possible [6], it requires an incredible amount of shower simulations. With current techniques, it is nearly impossible to study the performance of such a reconstruction approach.

A much faster but still accurate approach to simulations is crucial. The new technique of template synthesis [11] is based on a re-weighting scheme that allows the generation of showers with arbitrary longitudinal profiles from one origin shower. Alternatively, the fast macroscopic code MGMR3D, can be used to reconstruct shower parameters including X_{max} [12].

Reconstruction of the L-parameter offers new possibilities to constrain the mass composition. The right panel of Fig. 3 shows the distribution of L for sets of 1500 showers that were simulated with CONEX for five different elements and three hadronic interaction models (EPOS-LHC, QGSJETII-04, and Sibyll 2.3d). The most pronounced variations are in the high-L tails of the distribution, which is largest for Helium and smallest for Iron. The fact that not protons but Helium nuclei have the highest L-values, makes it possible to isolate proton fractions in arbitrary compositions.

The right panel of Fig. 3 contains data points that correspond to arbitrary compositions. Each point contains 1500 showers with varying fractions of protons, Helium, Carbon, Silicon, and Iron. The proton fraction is color-coded. Moving from Iron to Helium, both the average X_{max} and the fraction of high-L showers increases. However, for protons X_{max} is still increasing, while there are less high-L showers. This allows a direct reconstruction of the proton fraction, which would be a powerful instrument to study the transition from Galactic to extragalactic sources.
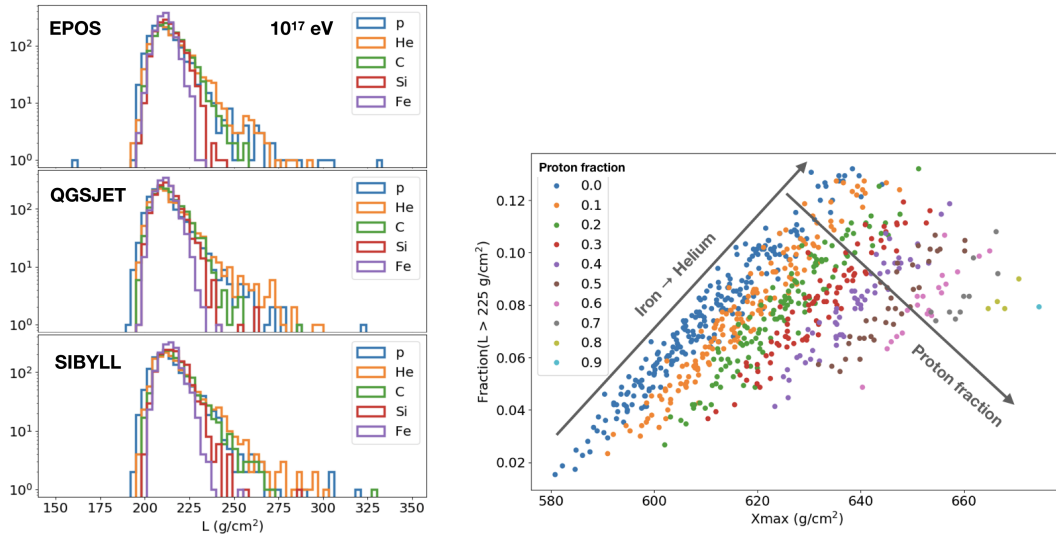
Figure 3: Left: Histograms of L for 10^{17} eV showers from different primaries for three different hadronic interaction models. The tail of the distribution towards higher values of L is largest for Helium and smallest for Iron. Right: Each dot represents a set of 1500 showers with a unique ratio of elements. The fraction of proton showers in the set is color-coded. The horizontal axis shows the mean X_{max} of the data sets, and the vertical axis shows the fraction of showers with an L-value exceeding 225 g/cm^2.

5. PeV gamma rays

The discovery of PeV gamma rays by LHAASO [14] has made the search for similar sources in the Southern sky a high priority. In principle, the SKA would be able to detect one or a few PeV gamma rays per year from a source like LHAASO J2032+4102. However, the detection of radio signals from PeV air showers is extremely challenging. Since the radiation mechanism is coherent, the radiated power scales with the square of the number of charges, and thus the primary energy.

The detection of PeV gamma-rays is in essence possible with the SKA when interferometric techniques are employed. The left panel of Fig. 4 shows the radio pulse of a 1 PeV gamma-ray shower. The SKA antenna model has been applied but the phase response has been corrected. In practice, correction of the phase response can be done in offline processing. Alternatively, for online triggering, matched filtering could be used to achieve similar signal-to-noise ratios (SNRs). The grey curve in the background is simulated background. The 150-350 MHz band was chosen to optimize the SNR, which is still only 0.27 for an optimal antenna position (near the Cherenkov cone).

The SNR can be improved by beamforming groups of antennas. A natural choice is to form beams with 256-antenna stations, resulting in an improvement on the SNR of a factor ∼ 16, as shown in the right panel of Fig. 4. While an SNR of ~4 implies that the gamma-ray shower is detectable, it will be challenging to design a robust triggering strategy.

The vast amount of data stored per trigger (readout of buffers of thousands of antennas) implies that it is unfeasible to trigger on all PeV showers. The cosmic-ray background can be reduced by accepting only triggers from the direction of a candidate source. The angular resolution of the beam is roughly λ/D, where λ is the central observation wavelength, and D the diameter of the area in
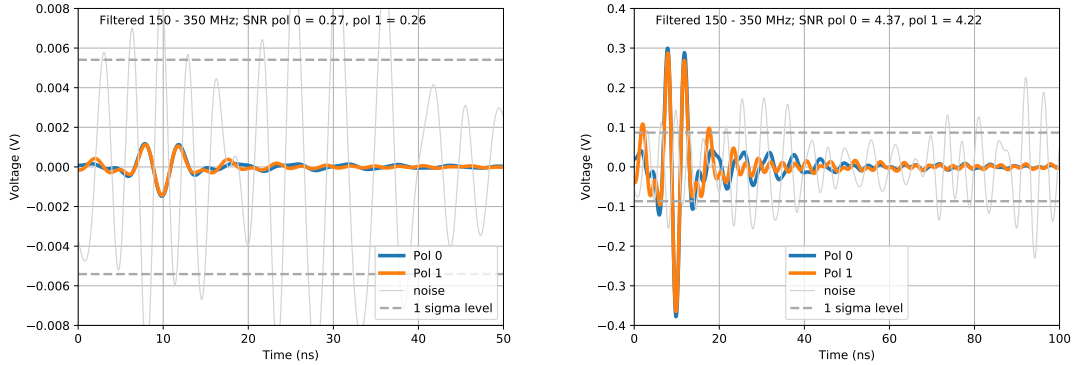
Figure 4: Left: Simulated radio pulse of a 1 PeV gamma-ray shower in the 150-350 MHz range. The antenna position is near the Cherenkov cone where the signal is expected to be strongest. The grey curve is simulated background and the dashed lines indicate the one sigma noise level. Right: Forming beams with 256 antennas will potentially improve the signal-to-noise ratio by a factor ~ 16.

which antennas are combined into a beam.

An acceptable trigger rate can be achieved by forming narrow beams in the direction of candidate sources, but only if triggers on radio noise can be suppressed. This could be achieved by only accepting radio triggers that coincide with a signal in two or more particle detectors.

The study of the feasibility of gamma-ray detection with the SKA is ongoing. The large amount of simulations is again a challenging factor. To simulate the effect of beamforming, the radio signal has to be accurately simulated for thousands of antenna positions. This has only recently become possible with the development of a new pulse interpolation method [15].

6. Conclusion

The SKA will be able to observe air showers in the sub-ankle energy range with unprecedented precision. It will have unique capabilities that complement other cosmic-ray observatories. Besides obtaining high-resolution X_{max} reconstructions, the high antenna density will also allow us to constrain other parameters of the longitudinal shower development such as the shower length L, which has unique information on the cosmic-ray mass composition. In addition, the observatory can in principle detect PeV gamma-rays, although triggering is a large challenge. Faster simulation methods are being developed to study these possibilities in further detail. An 8-station particle detector array is readied to be deployed later this year at the MWA, near the SKA site.

Acknowledgements

References

[1] S. Thoudam *et al.*, "Cosmic-ray energy spectrum and composition up to the ankle: the case for a second Galactic component", *Astron. & Astrophys.*, **595** A33 (2016)

[2] J. Bray *et al.*, "The SKA particle array prototype: The first particle detector at the Murchison Radio-astronomy Observatory", *NIMPA* **973**, article id. 164168 (2020)

[3] J. Bray, R. Ekers, and P. Roberts, "Noise statistics in a fast digital radio receiver: the Bedlam backend for the Parkes radio telescope", *Experimental Astronomy*, **36**, Issue 1-2 (2013)

[4] A. Williamson *et al.*, "An Ultra-High Time Resolution Cosmic-Ray Detection Mode for the Murchison Widefield Array", *J. of Astr. Instr.*, **10**, Issue 1, id. 2150003 (2021).

[5] S. Buitink *et al.*, "Method for high precision reconstruction of air shower $X_{\max}$ using two-dimensional radio intensity profiles", *Phys. Rev. D* **90** 082003 (2014)

[6] A. Corstanje *et al.*, "Prospects for measuring the longitudinal particle distribution of cosmic-ray air showers with SKA", **PoS(ARENA2022)024** *Santiago de Compostela, Spain* (2023).

[7] A. Corstanje *et al.*, Depth of shower maximum and mass composition of cosmic rays from 50 PeV to 2 EeV measured with the LOFAR radio telescope, *Phys. Rev. D* 103, 102006 (2021).

[8] B. Pont *et al.* **[Pierre Auger Observatory]**, "The depth of the shower maximum of air showers measured with AERA", **PoS ICRC2021** (2021).

[9] K. Mulrey *et al.*, "Cross-calibrating the energy scales of cosmic-ray experiments using a portable radio array", **PoS(ICRC2021)414** (2021).

[10] S. Andringa, R. Conceição, and M. Pimenta, "Mass composition and cross-section from the shape of cosmic ray shower longitudinal profiles", *Astroparticle Physics* **34** (2011).

[11] M. Desmet *et al.*, "Template synthesis approach for radio emission from extensive air showers", *submitted to Phys. Rev. D*, `arxiv.org/abs/2307.02939` (2023).

[12] P. Mitra *et al.*, "Reconstructing Air Shower Parameters with MGMR3D", *submitted* `arxiv.org/abs/2307.04242`

[13] S. Buitink *et al.*, "Constraining the cosmic-ray mass composition by measuring the shower length with SKA", **PoS(ARENA2022)046**, *Santiago de Compostela, Spain* (2023).

[14] Z. Cao *et al.* **[LHAASO]**, "Ultrahigh-energy photons up to 1.4 petaelectronvolts from 12 gamma-ray Galactic sources", *Nature* **594** (2021).

[15] A. Corstanje *et al.*, "A high-precision interpolation method for pulsed radio signals from cosmic-ray air showers", *submitted to JINST*, `arxiv.org/abs/2306.13514` (2023).